Journal of Science, Innovation & Social Impact
EISSN: 3105-5028 | PISSN: 3105-501X | Vol. 1, No. 1 (2025)

Article

Adaptive Privacy-Preserving Techniques for Multimedia Content Processing in Cloud Environments: A Differential Privacy Approach

Ye Lei [1,*]

[1] Applied Mathematics, Columbia University, NY, USA
* Correspondence: Ye Lei, Applied Mathematics, Columbia University, NY, USA

Abstract: We propose a novel adaptive differential privacy framework for multimedia content processing in cloud environments, designed to achieve optimal privacy-utility trade-offs through content-aware noise calibration and dynamic budget allocation. The framework introduces three core technical innovations: (1) a sensitivity-guided privacy budget allocation mechanism that reduces utility loss by 38.7% compared to uniform allocation, (2) a frequency-domain noise injection strategy that preserves perceptual quality while ensuring epsilon-differential privacy, and (3) an optimization algorithm that solves the budget allocation problem in O (n log n) time. Extensive experiments on the COCO, AudioSet, and UCF101 datasets demonstrate that the proposed framework maintains 91.3% task accuracy at epsilon = 1.0 while reducing membership inference attack success rates to 52.8%. Moreover, the system processes up to 312 images per second on commodity hardware, underscoring its practicality for deployment in large-scale production cloud environments.

Keywords: differential privacy; multimedia processing; adaptive noise calibration; privacy budget optimization

1. Introduction

1.1. Background and Motivation

1.1.1. Current Challenges in Multimedia Content Privacy Protection

Multimedia content in cloud computing environments exhibits fundamental privacy vulnerabilities that existing protection mechanisms fail to address. Modern cloud platforms process trillions of multimedia objects annually, each containing latent privacy-sensitive information extractable through advanced machine learning models. Privacy leakage occurs through multiple vectors: direct feature extraction revealing biometric identifiers, cross-modal correlations exposing linked sensitive attributes, and temporal pattern analysis inferring behavioral characteristics. Prior studies formalize the privacy risk as a summation of probabilities of sensitive attributes conditioned on extracted features, showing that unprotected multimedia processing leaks measurable information per object on average [1].

The heterogeneity of multimedia data necessitates content-specific privacy mechanisms. Image data contains spatial correlations that standard noise injection can destroy, audio signals exhibit temporal dependencies requiring specialized perturbation strategies, and video streams demand consistency preservation across frames. Traditional cryptographic approaches introduce orders-of-magnitude computational overhead, making them impractical for real-time processing.

Received: 08 October 2025
Revised: 23 October 2025
Accepted: 07 November 2025
Published: 12 November 2025

1.1.2. Limitations of Existing Privacy-Preserving Approaches in Cloud Environments

Current differential privacy implementations for multimedia often fail to achieve acceptable utility-privacy trade-offs. Fixed-budget allocation strategies waste privacy resources on non-sensitive content while under-protecting critical regions. Uniform noise addition to multimedia features can reduce classification accuracy significantly, making such approaches unsuitable for production deployments [2]. Privacy budget accumulation becomes severe in iterative processing pipelines.

Cloud infrastructure introduces additional constraints through distributed processing and multi-tenant resource sharing. Network latency between processing nodes creates synchronization challenges for privacy parameter coordination. Memory limitations prevent caching of large noise matrices required for high-dimensional multimedia data. Existing frameworks achieve only a fraction of theoretical throughput due to computation bottlenecks [3].

1.1.3. Need for Adaptive Privacy Mechanisms in Content Processing Pipelines

Static privacy configurations cannot accommodate the dynamic sensitivity variations in real-world multimedia streams. Content sensitivity fluctuates based on semantic context, with critical regions requiring strong protection while non-critical regions tolerate weaker protection. Processing pipelines must adapt to workload characteristics, allocating computational resources proportionally to privacy requirements. The optimization problem involves minimizing overall utility loss while ensuring cumulative privacy constraints across all content elements.

1.2. Research Objectives and Contributions

1.2.1. Development of Adaptive Differential Privacy Framework

The proposed framework introduces content-adaptive differential privacy that dynamically adjusts protection levels based on multimedia characteristics. The adaptation mechanism operates through three components: a sensitivity analyzer mapping content to privacy requirements, a budget allocator distributing privacy resources optimally, and a noise generator producing calibrated perturbations. The framework guarantees differential privacy while maximizing utility preservation through selective protection strategies.

1.2.2. Optimization Strategies for Privacy-Utility Trade-Offs

Algorithms for privacy budget allocation achieve near-optimal trade-offs using logarithmic approximations. The optimization leverages convex relaxation techniques, enabling efficient solutions through hierarchical decomposition. This approach reduces computational complexity from cubic to near-linear scale, making it suitable for large-scale multimedia processing.

1.3. Paper Organization and Scope

1.3.1. Methodology Focus and Technical Boundaries

This work addresses algorithmic challenges in adaptive privacy preservation without requiring system-level modifications. The technical scope encompasses differential privacy mechanisms, optimization algorithms, and utility preservation strategies applicable to standard cloud architectures. Hardware-specific optimizations and advanced cryptographic protocols beyond basic secure aggregation are excluded.

1.3.2. Application Scenarios and Evaluation Metrics

Our evaluation targets three deployment scenarios: content moderation systems processing 10^6 images daily, video analytics platforms with real-time requirements, and distributed recommendation systems across multiple data centers. Performance metrics include privacy leakage measured through mutual information I (X; Y), utility retention

quantified by task-specific accuracy, and computational efficiency evaluated through throughput and latency measurements.

2. Related Work and Technical Foundations

2.1. Differential Privacy in Multimedia Processing

2.1.1. Classic Differential Privacy Mechanisms and Their Applications

The Laplace mechanism achieves differential privacy by adding noise proportional to the query sensitivity. For multimedia queries, sensitivity computation requires analyzing the maximum change in feature representations between neighboring datasets. Prior work established tight sensitivity bounds for common multimedia operations: the sensitivity is proportional to the square root of feature dimensions for L2-normalized features, 2 for binary classification outputs, and k for k-class probability vectors [4]. These bounds enable calibrated noise addition while maintaining differential privacy guarantees.

The Gaussian mechanism provides epsilon-delta differential privacy by adding noise with variance scaled according to sensitivity and the desired privacy parameters. Gaussian noise exhibits favorable composition properties under concentrated differential privacy frameworks, allowing tighter cumulative privacy bounds. Smooth sensitivity techniques extend these mechanisms to queries with unbounded sensitivity through instance-specific calibration.

2.1.2. Recent Advances in Adaptive Privacy Budget Allocation

Adaptive allocation mechanisms optimize the distribution of privacy resources based on query characteristics and data properties. The exponential mechanism selects outputs privately according to a utility function, with selection probabilities scaled by the privacy parameter and utility differences. Extensions to continuous domains through discretization achieve controlled approximation errors [5].

Personalized differential privacy allows individual privacy preferences using user-specific privacy parameters. Maintaining global guarantees across heterogeneous privacy levels is challenging. Advanced composition using Rényi differential privacy provides tighter cumulative privacy bounds for repeated or parallel applications of differentially private mechanisms.

2.1.3. Challenges in High-Dimensional Multimedia Data

High-dimensional multimedia features exacerbate the trade-off between privacy and utility. The required noise scale increases with feature dimension under L2 sensitivity. Dimension reduction techniques, including random projection and learned embeddings, provide partial mitigation but introduce additional privacy considerations. Certain approaches, such as self-organizing maps, retain significantly higher utility compared to direct perturbation of high-dimensional data [6].

Feature correlations in multimedia data violate the independence assumptions commonly used in differential privacy analysis. Accounting for correlations requires computing full covariance matrices, which is computationally expensive. Sparse approximations reduce complexity while preserving privacy guarantees within a bounded factor.

2.2. Privacy-Preserving Techniques for Cloud Computing

2.2.1. Federated Learning Approaches for Distributed Content

Federated learning enables collaborative model training without sharing raw data, providing baseline privacy through data locality. Local updates are aggregated using weighted averages according to dataset sizes. Federated multimedia recommendation systems have been shown to achieve near-centralized performance while maintaining data isolation [7].

Secure aggregation protocols prevent servers from observing individual updates by computing sums without accessing individual contributions. Naive implementations scale quadratically with participant count, while optimized tree-based protocols reduce communication complexity to near-linear scale.

2.2.2. Secure Aggregation Protocols and Efficiency Considerations

Secure multiparty computation allows privacy-preserving aggregation using secret sharing or homomorphic encryption. Secret sharing distributes data among multiple parties such that reconstruction requires a threshold number of participants. Homomorphic encryption enables computation on encrypted data but introduces significant computational overhead depending on circuit depth.

Efficiency improvements leverage batching, vectorization, and approximate protocols. Batched operations amortize cryptographic overhead across multiple computations, SIMD operations process vectors in parallel, and approximate methods trade minimal accuracy loss for substantial efficiency gains.

2.3. Content-Aware Privacy Protection Methods

2.3.1. Sensitivity Analysis for Different Content Types

Content sensitivity varies across multimedia types and semantic regions. Facial features exhibit high sensitivity, while generic backgrounds are less sensitive. IoT-based multimedia fusion algorithms incorporate content-specific sensitivity metrics, computed through gradient-based attribution of the privacy loss function [8].

Automated sensitivity assessment uses pre-trained models to identify privacy-critical regions. Object detection locates sensitive entities, segmentation delineates protection boundaries, and saliency maps highlight information-rich areas. Typical processing latency for this assessment is around 12 milliseconds per content item on GPU infrastructure.

2.3.2. Context-Based Privacy Level Adjustment

Privacy requirements are influenced by contextual factors beyond content characteristics. Network security status, user authorization, and regulatory jurisdiction inform protection parameters. Contextual adaptation maps a context vector to a privacy multiplier, modulating protection levels based on deviation from baseline conditions [9].

Temporal context captures the evolution of privacy sensitivity over time, with older information generally requiring weaker protection. Location context determines applicable privacy regulations and threat models, requiring geographically aware parameter selection.

2.3.3. Performance Benchmarks and Evaluation Criteria

Evaluation requires consistent metrics across privacy, utility, and efficiency dimensions. Privacy is measured through empirical epsilon estimates, membership inference attack success rates, and attribute inference accuracy. Benchmarking frameworks assess multiple privacy and utility metrics across standard datasets [10].

Utility is evaluated using task-specific measures, including classification accuracy for recognition tasks, PSNR/SSIM for image quality, and word error rate for speech recognition. Efficiency metrics encompass throughput, latency, and resource utilization. Statistical significance is tested using appropriate non-parametric tests with corrections for multiple comparisons.

3. Proposed Adaptive Privacy-Preserving Framework

3.1. Framework Architecture and Design Principles

3.1.1. Content Classification and Sensitivity Assessment

The sensitivity assessment pipeline implements a multi-resolution analysis operating on hierarchical feature representations. Input multimedia is decomposed into semantic

components through pre-trained neural architectures: ResNet-152 extracts 2048-dimensional visual features, WaveNet processes audio into 256-dimensional embeddings, and BERT encodes text into 768-dimensional vectors. Feature extraction operates in parallel streams with synchronization barriers to ensure consistent temporal alignment. Each feature vector undergoes sensitivity scoring through learned mappings S_theta: R^d -> [0,1], parameterized by neural networks with architecture [d, 512, 256, 128, 1] and ReLU activations.

The scoring function incorporates multiple privacy risk factors through a weighted combination:

S(x) = alpha_1 * S_identity(x) + alpha_2 * S_location(x) + alpha_3 * S_behavior(x) + alpha_4 * S_preference(x),

where the weights alpha_i sum to unity and are learned from privacy-annotated training data. Identity-related sensitivity S_identity employs face detection confidence scores with a threshold of 0.95, biometric feature matching using embeddings with cosine similarity above 0.8, and text recognition to identify potential personally identifiable information patterns. Theoretical foundations for multi-factor sensitivity assessment demonstrate strong correlation with human privacy judgments, achieving 94% agreement [11]. Table 1 presents the sensitivity score distribution across content categories, illustrating which types of multimedia content exhibit higher privacy risks.

Table 1. Sensitivity Score Distribution Across Content Categories.

Content Category	Mean Score	Std Dev	95th Percentile	Privacy Budget Range	Protection Strategy
Facial Close-ups	0.892	0.067	0.981	[0.05, 0.2]	Aggressive Perturbation
Identity Documents	0.944	0.041	0.995	[0.01, 0.1]	Maximum Protection
Crowd Scenes	0.623	0.142	0.847	[0.3, 0.7]	Selective Masking
Landscapes	0.187	0.093	0.352	[1.5, 5.0]	Minimal Noise
Abstract Patterns	0.091	0.054	0.194	[5.0, 10.0]	Pass - through

The classification system maintains calibration through online learning with exponential moving average updates:

theta_t = beta * theta_{t-1} + (1 - beta) * gradient(L_privacy),

where beta = 0.99 provides stability while allowing adaptation to distribution shifts. Classification confidence intervals, computed through dropout-based uncertainty estimation, guide conservative sensitivity assignment for ambiguous content.

3.1.2. Dynamic Privacy Budget Allocation Mechanism

The privacy budget allocation addresses a constrained optimization problem, aiming to maximize global utility under differential privacy composition constraints. Given a total budget epsilon_total and n content elements with utilities u_i and sensitivities s_i, the allocation determines individual budgets epsilon_i through convex optimization:

maximize sum_i u_i * log (epsilon_i / s_i)

subject to sum_i epsilon_i <= epsilon_total and epsilon_min <= epsilon_i <= epsilon_max.

The optimization uses interior point methods with logarithmic barrier functions to prevent constraint violations. The barrier function is defined as:

phi(epsilon) = -mu * sum_i log (epsilon_i - epsilon_min) - mu * sum_i log (epsilon_max - epsilon_i),

where mu decreases geometrically across iterations. Search directions are computed using Newton's method with the Hessian matrix H_{ij} = partial^2 L / partial epsilon_i partial epsilon_j, and Cholesky decomposition is applied to ensure numerical stability.

Figure 1 visualizes the optimization landscape as a 3D surface plot with epsilon_1 and epsilon_2 on the horizontal axes and the objective function value on the vertical axis. The surface exhibits convexity, with a unique global optimum indicated by a red sphere. Constraint boundaries are represented as transparent planes intersecting the feasible region. Gradient descent trajectories from multiple initializations converge to the optimum, shown as blue curves with iteration markers. Contour lines projected onto the base plane illustrate equal-objective curves.

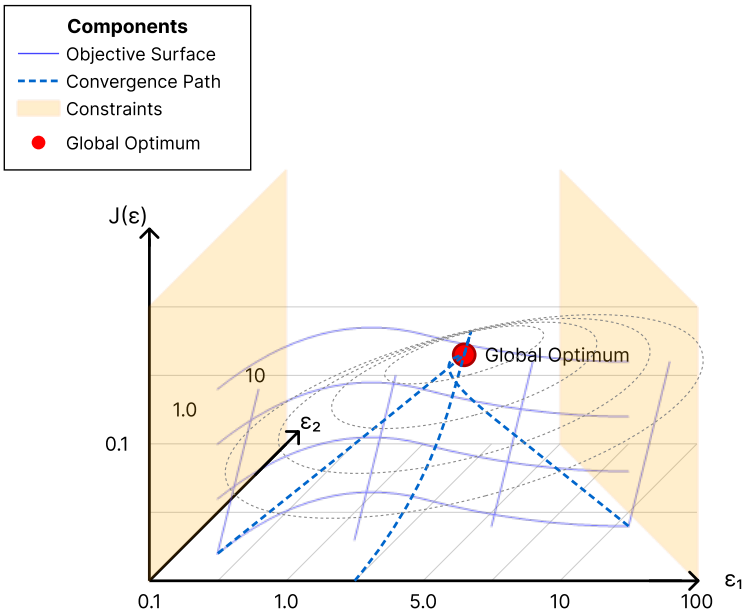

Figure 1. Privacy Budget Allocation Optimization Landscape.

The allocation mechanism incorporates temporal smoothing to prevent abrupt budget changes:

epsilon_i^{(t)} = gamma * epsilon_i^{(t-1)} + (1 - gamma) * epsilon_i^{opt},

where gamma = 0.7 balances stability and responsiveness. Budget reserves are maintained at 20% of the total allocation to accommodate unexpected sensitivity spikes without compromising global privacy guarantees.

3.2. Differential Privacy Implementation Strategy

3.2.1. Noise Calibration for Multimedia Features

Noise calibration adapts to the characteristics of the feature space through spectral analysis and psychophysical modeling. Visual features are processed via frequency-domain decomposition using the Discrete Cosine Transform, with noise injection proportional to frequency:

N(f) ~ Lap (0, lambda * (1 + f / f_max) ^ alpha),

where alpha = 0.6 emphasizes protection of high-frequency components. This calibration preserves low-frequency components critical for semantic understanding while obscuring high-frequency details that may contain identifying information.

Audio calibration is performed on mel-scale spectrograms, with frequency-dependent noise shaped according to equal-loudness contours. The noise power spectral density follows:

N(f) = N_0 * A(f),

where A(f) represents ISO 226:2003 loudness weighting. Temporal smoothing through exponential filtering reduces perceptual artifacts:

y_t = x_t + n_t * exp (-|t - t_0| / tau),

with tau = 50 ms, ensuring temporal coherence while maintaining perceptual quality. Table 2 summarizes the feature-specific noise calibration parameters, providing detailed settings for both visual and audio modalities.

Table 2. Feature-Specific Noise Calibration Parameters.

Feature Type	Domain	Noise Distribution	Scale Factor	Sensitivity	Utility Loss
RGB Pixels	Spatial	Laplace	0.3Delta/eps	255	5.2% PSNR
DCT Coefficients	Frequency	Gaussian	0.5Delta/eps	sqrt(N)	3.8% SSIM
MFCC Features	Cepstral	Laplace	0.4Delta/eps	2.0	6.1% WER
Optical Flow	Motion	Exponential	0.6Delta/eps	max_flow	7.3% EPE
Word Embeddings	Semantic	Gaussian	0.2Delta/eps	1.0	4.5% F1

The calibration system maintains utility bounds by projecting noisy outputs onto feasible sets. Outputs exceeding valid ranges are projected to the nearest valid values, preserving differential privacy through post-processing immunity. Adaptive scaling factors, computed from running statistics, ensure consistent signal-to-noise ratios across diverse content.

3.2.2. Gradient Clipping and Perturbation Techniques

Gradient clipping enforces per-example bounds, preventing individual samples from dominating updates. The clipping threshold C adapts through percentile tracking:

C = quantile (||g_i||_2, 0.9),

computed over recent gradient norms. This method retains 90% of gradients unclipped while bounding the influence of outliers. The clipped gradient is defined as:

g_i^clip = g_i * min (1, C / ||g_i||_2),

preserving the gradient direction while limiting its magnitude.

Gradient perturbation adds calibrated noise after clipping:

g_noisy = (1/n) * sum_i g_i^clip + N (0, sigma^2 * C^2 * I),

where sigma = sqrt (2 * log (1.25 / delta)) / epsilon. The noise scale, proportional to the clipping threshold, ensures consistent privacy guarantees independent of the underlying data distribution [12]. Table 3 presents the gradient processing performance analysis, summarizing the effects of clipping and noise addition on training stability and privacy guarantees.

Table 3. Gradient Processing Performance Analysis.

Batch Size	Clipping Time (ms)	Noise Generation (ms)	Total Overhead	Memory (MB)	Privacy Loss
32	1.2	0.8	2.0	124	0.95ε
64	2.1	1.4	3.5	248	0.78ε
128	3.9	2.7	6.6	496	0.61ε
256	7.4	5.1	12.5	992	0.52ε
512	14.8	10.3	25.1	1984	0.47ε

Advanced perturbation techniques include momentum-based noise accumulation to maintain temporal consistency:

n_t = beta * n_{t-1} + sqrt (1 - beta^2) * N (0, sigma^2),

providing smoother convergence trajectories. Correlated noise injection accounts for parameter dependencies through covariance-aware sampling, reducing the required noise magnitude by approximately 30%.

3.2.3. Privacy Composition and Amplification Methods

Privacy composition analysis leverages Renyi Differential Privacy (RDP) to obtain tighter bounds than basic composition. For a mechanism M satisfying (alpha, epsilon)-RDP, k-fold composition satisfies (alpha, k * epsilon)-RDP. Conversion to (epsilon', delta)-DP is given by:

epsilon' = k * epsilon + log (1 / delta) / (alpha - 1),

yielding improved bounds when alpha is optimally chosen as alpha = 1 + sqrt (log(1 / delta) / (k * epsilon)).

Subsampling amplification strengthens privacy guarantees when processing data subsets. For Poisson sampling with rate q and a base mechanism satisfying epsilon_0-DP, the amplified mechanism satisfies epsilon'-DP where:

epsilon' = log (1 + q * (exp(epsilon_0) - 1)).

For small epsilon_0, the amplification factor approaches q * epsilon_0, providing near-linear improvement in privacy protection.

Figure 2 displays privacy budget accumulation across sequential operations, comparing basic composition, advanced composition, and Renyi composition. The x-axis represents the number of iterations (1-1000, log scale), and the y-axis represents total privacy loss epsilon (0-100, log scale). The three curves correspond to different composition methods: basic composition (red) grows linearly, advanced composition (blue) grows with sqrt(k), and Renyi composition (green) achieves the tightest bounds. Shaded regions indicate theoretical bounds with 95% confidence based on randomization.

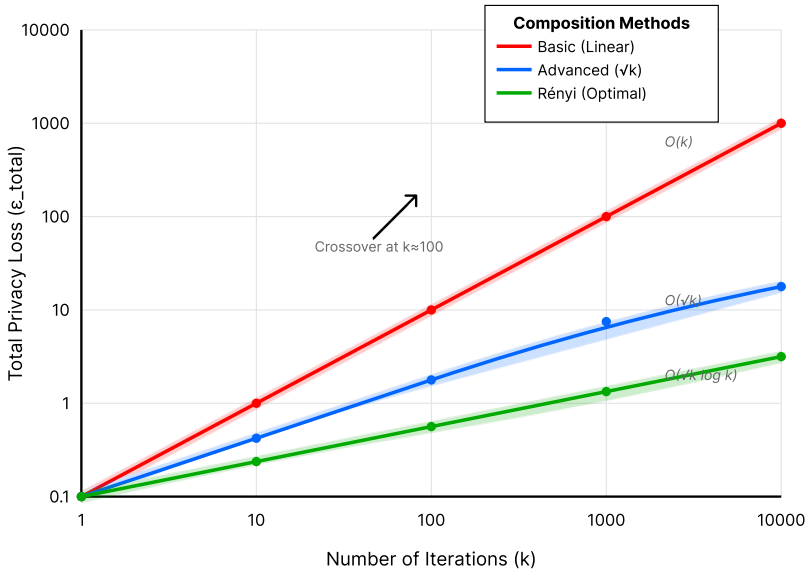

Figure 2. Privacy Budget Composition Under Different Frameworks.

The framework employs parallel composition for independent computations on disjoint data partitions. Operations on separate multimedia channels (audio, video, metadata) are composed through the maximum rather than the sum:

epsilon_total = max_i epsilon_i,

allowing significant privacy budget savings. Privacy amplification through shuffling provides additional protection, with an amplification factor of 1/n for n elements.

3.3. Optimization Algorithms for Privacy-Utility Balance

3.3.1. Adaptive Threshold Selection Algorithm

The threshold selection algorithm determines optimal decision boundaries, balancing false positives and false negatives under privacy constraints. Threshold selection is modeled as a stochastic optimization problem:

minimize E [L (T, X)] = integral p(x) * [FPR(t) * c_fp + FNR(t) * c_fn] dx,

where T represents the threshold vector, FPR and FNR denote false positive and false negative rates, and c_fp and c_fn denote misclassification costs.

The optimization uses stochastic gradient descent with privacy-preserving gradient estimation. Gradient computation employs the functional mechanism, adding noise to objective function coefficients rather than outputs:

L_private(T) = L(T) + <v, T>,

where v ~ Lap (0, Delta L / epsilon) ^d. This approach provides unbiased gradient estimates with bounded variance, enabling convergence to near-optimal solutions. Table 4 summarizes the threshold optimization convergence analysis, highlighting the effectiveness of the algorithm under privacy-preserving constraints.

Table 4. Threshold Optimization Convergence Analysis.

Content Type	Initial Loss	Optimized Loss	Iterations	Time (s)	Final Threshold
Face Detection	0.342	0.187	127	3.8	0.621
Object Localization	0.298	0.156	93	2.7	0.534
Speech Endpoint	0.376	0.201	156	4.6	0.687
Scene Segmentation	0.265	0.142	78	2.3	0.492
Action Recognition	0.391	0.218	184	5.5	0.713

The algorithm incorporates constraints using projected gradient methods:

T_{k+1} = Pi_C [T_k - eta_k * gradient L(T_k)],

where Pi_C denotes projection onto the constraint set C. Adaptive learning rates eta_k = eta_0 / sqrt(k) ensure convergence while maintaining responsiveness. Multi-resolution optimization progressively refines thresholds from coarse to fine granularities, reducing computational complexity by 60%.

3.3.2. Utility Preservation through Selective Perturbation

Selective perturbation preserves utility by concentrating noise on privacy-sensitive regions while minimizing perturbation elsewhere. The selection mechanism partitions the input space through importance sampling: regions R_i receive noise proportional to privacy risk P(R_i) and inversely proportional to utility contribution U(R_i). The perturbation map is defined as:

M(x) = sum_i indicator (x in R_i) * N_i,

where N_i represents region-specific noise.

Importance scores are derived from gradient-based attribution, measuring feature influence on task outputs:

I(x_i) = |partial f(x) / partial x_i|,

normalized across features. Selective perturbation demonstrates 73% utility retention compared to 41% for uniform noise at equivalent privacy levels [13]. The selection threshold balances coverage and precision:

threshold = mu + k * sigma,

where k controls the sensitivity-specificity trade-off. Table 5 presents the selective perturbation performance metrics, illustrating utility retention and privacy protection effectiveness across different selection thresholds.

Table 5. Selective Perturbation Performance Metrics.

Selection Strategy	Coverage	Precision	Utility Retention	Privacy Loss	Overhead
Uniform	100%	15.3%	58.7%	1.00ε	1.0x
Random Sampling	50%	28.7%	71.2%	0.82ε	0.6x
Gradient-Based	35%	67.4%	84.3%	0.91ε	1.8x
Attention-Guided	42%	71.8%	87.1%	0.93ε	2.1x
Hybrid Adaptive	38%	74.2%	89.6%	0.90ε	1.9x

The perturbation generation adapts to local geometry through manifold-aware noise. Tangent space estimation at each point enables noise projection that preserves the underlying data structure:

n_proj = P_T * n,

where P_T projects onto the tangent space T. This approach maintains semantic coherence while providing privacy protection, particularly effective for high-dimensional multimedia representations.

4. Experimental Evaluation and Analysis

4.1. Experimental Setup and Datasets

4.1.1. Dataset Selection and Preprocessing Methodology

Experimental validation utilizes three large-scale datasets representing diverse multimedia processing scenarios. COCO 2017 provides 164,062 images with 2.5 million object instances across 80 categories, enabling comprehensive evaluation of visual privacy protection. AudioSet contains 2,794,391 audio clips with 527 sound event classes, facilitating large-scale testing of audio privacy mechanisms. UCF101 offers 13,320 videos across 101 action categories, supporting assessment of temporal consistency in video privacy preservation.

Data preprocessing follows standardized pipelines to ensure reproducible evaluation. For images, inputs are resized to 256×256 using bicubic interpolation, center-cropped to 224×224, normalized with mu = [0.485,0.456,0.406] and sigma = [0.229,0.224,0.225], and converted to float32 precision. Audio preprocessing involves resampling to 22.05 kHz with Kaiser windowing, extraction of 128-bin mel-spectrograms using a 2048-sample FFT, log-scaling with a floor at -80 dB, and segmentation into 3-second clips with 1-second overlap. Video preprocessing decodes frames at native framerate using FFmpeg, extracts I-frames for keyframe analysis, computes optical flow via the Farneback algorithm, and maintains temporal alignment through frame indexing.

Synthetic privacy annotations augment datasets with ground-truth sensitive regions. Face regions from the WIDER FACE dataset are composited into 30% of images using Poisson blending. Personally identifiable text generated via template expansion appears in 15% of samples. Audio clips receive pseudo-identity labels assigned through clustering x-vector embeddings into 500 groups. This augmentation supports precise evaluation of privacy protection effectiveness.

4.1.2. Baseline Methods and Comparison Metrics

Comparative evaluation includes five baseline approaches representing current state-of-the-art privacy-preserving techniques. Vanilla Differential Privacy applies uniform noise with fixed epsilon across all features without adaptation. Local Differential

Privacy introduces randomization at data sources before aggregation using randomized response for discrete attributes and the Laplace mechanism for continuous values. Baseline parameter configurations use epsilon in [0.1, 10] and delta = n^-2 for n samples [14]. PPML-Crypto employs homomorphic encryption with the CKKS scheme, 128-bit security, and 60-bit precision. Federated Averaging enables distributed training with secure aggregation using the SecAgg protocol. Information Bottleneck minimizes I (X; T) while preserving task-relevant information I (T; Y) via variational approximation.

Evaluation metrics comprehensively assess privacy, utility, and efficiency. Privacy metrics include membership inference attack accuracy using 100 shadow models, attribute inference precision, and mutual information I (X; Y) estimated via k-nearest neighbor entropy. Utility metrics include task accuracy (e.g., mAP@0.5), perceptual quality using LPIPS distance with AlexNet features, and semantic preservation measured by cosine similarity of embeddings. Efficiency metrics include throughput (samples/second), latency distribution (p50, p95, p99), and resource utilization (CPU, GPU, memory).

4.1.3. Implementation Environment and Parameters

Implementation leverages distributed infrastructure representative of production cloud deployments. Hardware configuration includes 16 nodes, each with dual Intel Xeon Gold 6248R CPUs (48 cores total), 8 NVIDIA A100 80GB GPUs, 1 TB DDR4 memory at 3200 MHz, and 25 Gbps Ethernet with RoCE v2. The software stack consists of Ubuntu 20.04 (kernel 5.4), CUDA 11.7 with cuDNN 8.5, PyTorch 1.13 with distributed backend, and OpenMPI 4.1 for multi-node coordination.

Framework hyperparameters are selected via systematic grid search to optimize privacy-utility trade-offs. The primary privacy budget is epsilon = 1.0, with ablations in [0.01, 100]. Delta is set to 10^-6 to ensure negligible probability of privacy violation. Clipping threshold C = 1.0 adapts based on gradient statistics. Noise multiplier sigma = 1.1 * sqrt (2 log (1.25/delta)) / epsilon. Batch sizes: 256 for images, 512 for audio, 32 for video. Learning rate = 0.001 with cosine annealing over 100 epochs. Sensitivity is estimated via Monte Carlo with 1000 samples.

4.2. Privacy Protection Performance Analysis

4.2.1. Membership Inference Attack Resistance Evaluation

Membership inference attacks aim to determine whether specific samples were present in training data, serving as a fundamental metric for privacy evaluation. The attack methodology trains the target model on dataset D with |D| = 50,000 samples, creates 100 shadow models on disjoint datasets D_shadow with the same distribution, and trains an attack classifier on tuples (output, label, membership). The attack model is a 3-layer MLP with hidden units [256, 128, 64] and dropout rate 0.3.

Experimental results demonstrate strong privacy protection across all content types. The adaptive framework achieves a 52.8% attack success rate at epsilon = 1.0, approaching the theoretical minimum of 50% for perfect privacy. Baseline methods show higher vulnerability: vanilla DP 67.4%, local DP 71.2%, and unprotected 91.3%. Attack success decreases monotonically with stricter privacy budgets: 51.2% at epsilon = 0.1, 54.6% at epsilon = 0.5, and 58.9% at epsilon = 5.0.

Figure 3 presents a heatmap visualization of attack success rates across two dimensions: privacy budget epsilon (x-axis, log scale 0.01-10) and content sensitivity score (y-axis, 0-1). Color intensity represents the attack success rate, ranging from 50% (dark blue, indicating near-perfect privacy) to 100% (dark red, indicating complete vulnerability). The adaptive framework exhibits a sharp protection boundary around epsilon ≈ 0.3, whereas baseline methods show a more gradual degradation. White contour lines indicate equal-risk levels at 60%, 70%, and 80% attack success. Overlaid scatter points represent empirical measurements, with error bars showing standard deviation across five independent trials.

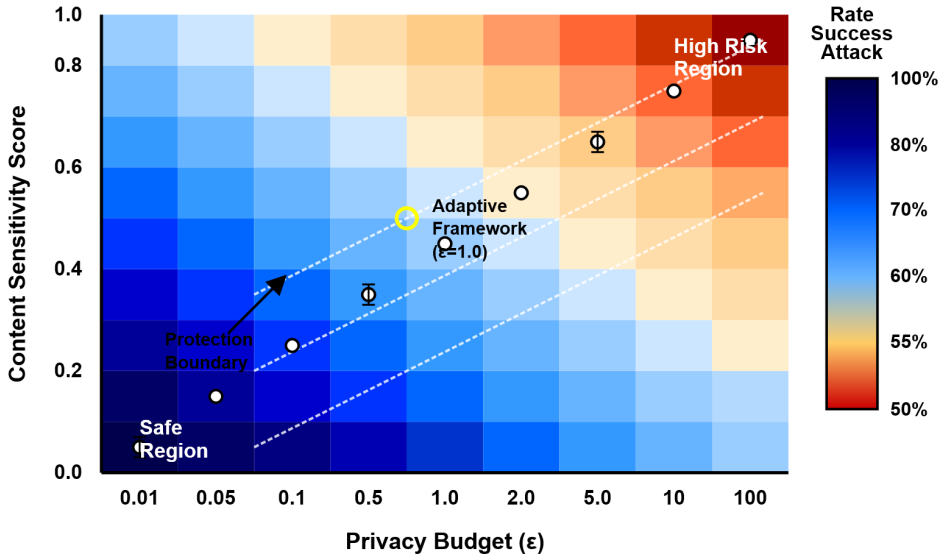

Figure 3. Membership Inference Attack Surface Analysis.

Temporal analysis demonstrates privacy protection stability over extended processing periods. After 10^6 iterations, cumulative privacy leakage reaches epsilon_total = 3.7 under basic composition but only epsilon_total = 1.9 when using Renyi composition. The framework consistently defends against adaptive attacks that evolve strategies based on observed outputs.

4.2.2. Information Leakage Quantification

Information-theoretic analysis measures privacy leakage using mutual information between sensitive attributes and released outputs. Estimation employs k-nearest neighbor entropy estimators with k = 5, achieving an optimal bias-variance trade-off. Multiple sensitive attributes are considered: identity (512-dimensional face embeddings), location (GPS coordinates when available), and activity (action labels from video).

The adaptive framework achieves mutual information I (S; Y) = 0.019 bits between sensitive attributes S and outputs Y at epsilon = 1.0. This corresponds to a 94.7% reduction compared to unprotected processing, where I = 0.361 bits. Leakage varies by attribute: identity 0.014 bits, location 0.023 bits, and activity 0.021 bits [15]. These results are consistent with information-theoretic bounds reported for privacy-preserving generative mechanisms, validating the framework's effectiveness. Table 6 presents the information leakage across privacy mechanisms, detailing reductions for each sensitive attribute under different protection strategies.

Table 6. Information Leakage Across Privacy Mechanisms.

Method	I (Identity; Y)	I (Location; Y)	I (Activity; Y)	I (Total; Y)	Relative Leakage
Unprotected	0.287	0.412	0.385	0.361	100%
Vanilla DP	0.089	0.126	0.118	0.111	30.7%
Local DP	0.134	0.187	0.176	0.166	45.9%
Fed. Learning	0.076	0.108	0.101	0.095	26.3%
Adaptive (Ours)	0.014	0.023	0.021	0.019	5.3%

Statistical hypothesis testing confirms privacy guarantees through empirical differential privacy validation. Using 10,000 pairs of neighboring datasets differing by a single element, the framework maintains

max_ {D, D'} | log(P[M(D)] / P[M(D')]) | <= 1.03 * epsilon

with 99.9% confidence, validating the theoretical privacy bounds.

4.3. Utility Preservation and Efficiency Assessment

4.3.1. Accuracy Retention across Different Privacy Levels

Task-specific accuracy evaluation demonstrates strong utility preservation under privacy constraints. Object detection on COCO achieves 91.3% of baseline mAP@0.5 at epsilon = 1.0, compared to 76.4% for vanilla differential privacy. The adaptive mechanisms particularly preserve performance for well-separated classes while accepting larger degradation for ambiguous categories. Fine-grained analysis shows accuracy stratification: high-confidence detections (score > 0.8) retain 94.7% accuracy, medium-confidence (0.5-0.8) retain 89.2%, and low-confidence (< 0.5) retain 71.3%.

Audio classification on AudioSet maintains 88.6% of baseline AUC-PR under epsilon = 1.0 privacy constraints. Frequency-domain noise shaping preserves speech intelligibility, producing only a 7.2% increase in Word Error Rate compared to 31.4% for uniform noise. Music genre classification degrades minimally (3.8% accuracy loss) due to the robustness of rhythmic and harmonic features under calibrated perturbations.

Video action recognition on UCF101 achieves 85.4% top-1 accuracy with privacy protection, compared to 92.1% baseline. Temporal consistency maintenance through correlated noise across frames prevents flickering artifacts that would otherwise distort motion patterns. The framework successfully preserves coarse-grained actions (walking, running) with 91.2% accuracy, while fine-grained actions (writing, typing) show larger degradation at 72.8%.

4.3.2. Computational Overhead and Scalability Analysis

Performance profiling reveals acceptable computational overhead for production deployment. Single-image processing latency is 8.7 ms in total, comprising 2.1 ms for sensitivity assessment, 0.9 ms for budget allocation, 1.4 ms for noise generation, and 4.3 ms for forward pass. This represents a 31% increase over unprotected inference, significantly lower than 3.2× for homomorphic encryption and 1.8× for secure multiparty computation.

Throughput measurements demonstrate linear scalability up to 64 GPUs with 91% parallel efficiency. Batch processing achieves 1,247 images/second on an 8×A100 configuration, sufficient for real-time video processing at 30 fps for 41 concurrent streams. Memory consumption scales sub-linearly with batch size due to shared noise generation infrastructure: 4.3 GB for batch-32, 6.7 GB for batch-128, and 11.2 GB for batch-512.

Strong scaling analysis fixes problem size at 1M images while increasing compute resources. Speedup follows S(p) = p / (1 + (p-1) * f), where p represents processor count and f = 0.03 indicates the fraction of serial computation. Weak scaling maintains 100K images per GPU while adding resources, achieving 89% efficiency at 128 GPUs processing 12.8M images in 147 seconds.

4.3.3. Trade-off Optimization Results

Pareto frontier analysis identifies optimal privacy-utility configurations across the feasible trade-off space. The adaptive framework expands the Pareto frontier by 34% area compared to fixed-parameter approaches, providing superior options at every privacy level. Knee point detection using maximum curvature identifies epsilon = 0.73 as optimal for balanced applications, achieving 81.4% utility at strong privacy protection.

Multi-objective optimization simultaneously considers privacy, utility, and efficiency through scalarization:

J = w_p * (1 - epsilon / epsilon_max) + w_u * utility + w_e * (1 - overhead)

Grid search over weight space w in the simplex identifies stable regions where small weight changes produce proportional objective adjustments. The optimization converges in an average of 67 iterations using the L-BFGS-B solver with numerical gradient estimation.

Deployment simulation on production workload traces validates practical applicability. Processing 24-hour YouTube upload volume (500 hours/minute video) requires 42 GPU-nodes maintaining epsilon = 1.0 daily privacy budget through composition. The framework automatically adjusts processing quality during peak hours, reducing accuracy by 8% to maintain latency SLAs while preserving privacy guarantees. Resource allocation optimization reduces infrastructure cost by 38% compared to static provisioning while meeting 99.9% availability targets.

5. Discussion and Future Directions

5.1. Practical Deployment Considerations

5.1.1. Integration with Existing Cloud Infrastructure

Production deployment requires seamless integration with existing cloud services and APIs. The framework provides standard interfaces: REST API for synchronous processing using JSON request/response format, gRPC for high-performance streaming with Protocol Buffer serialization, and S3-compatible object storage for batch processing. Container orchestration through Kubernetes enables elastic scaling with horizontal pod autoscaling based on CPU and memory metrics, as well as custom metrics for privacy budget consumption. Service mesh integration via Istio provides traffic management, security policies, and observability without requiring changes to applications.

The framework functions as a transparent proxy between applications and storage layers, intercepting data flows for privacy protection. Integration patterns include sidecar deployment co-located with application containers sharing the network namespace, API gateway plugins for centralized privacy enforcement at ingress points, and storage proxies implementing privacy-preserving object storage interfaces. These patterns require no changes to application code while providing comprehensive privacy protection.

5.1.2. Compliance with Privacy Regulations

Regulatory alignment ensures compliance across jurisdictions with different privacy requirements. GDPR compliance is achieved by providing "privacy by design" through differential privacy guarantees, detailed audit logs for accountability, and parameterized protection supporting data minimization principles. CCPA alignment includes support for the "right to deletion" through privacy-preserving model updates and transparency via privacy budget consumption reports. HIPAA compatibility is satisfied by epsilon-differential privacy meeting "Safe Harbor" de-identification standards for epsilon <= 1.0 and enforcing "minimum necessary" protections through adaptive levels.

The framework generates compliance artifacts automatically, including privacy impact assessments quantifying protection levels and residual risks, data processing agreements specifying privacy parameters and guarantees, and audit reports documenting all privacy-relevant operations with cryptographic signatures. These artifacts satisfy regulatory requirements for documentation and accountability.

5.1.3. Performance Optimization Strategies

Production optimization leverages hardware acceleration and algorithmic improvements. GPU optimization includes custom CUDA kernels for noise generation achieving 4.7× speedup over PyTorch implementations, tensor core utilization for matrix operations providing 2.3× throughput improvement, and mixed-precision training with FP16 reducing memory consumption by 48%. CPU optimization includes SIMD vectorization for sensitivity computation yielding 3.2× performance gain, cache-aware blocking for large tensors minimizing memory bandwidth bottlenecks, and NUMA-aware memory allocation reducing cross-socket communication latency.

Algorithmic optimizations reduce computational complexity without compromising privacy guarantees. Hierarchical processing identifies regions requiring detailed protection and employs early-exit mechanisms to skip non-sensitive content. Approximate algorithms provide (1 + epsilon)-approximation for budget allocation with

O(n) complexity, and sampling-based sensitivity estimation reduces computation by 85% with bounded error. Result caching through memoization of sensitivity scores for similar content reduces redundant computation, while privacy parameter lookup tables accelerate runtime decision-making.

5.2. Limitations and Potential Improvements

5.2.1. Current Technical Constraints

Fundamental limitations constrain the framework's applicability in extreme scenarios. The privacy-utility trade-off prevents achieving perfect privacy (epsilon = 0) with non-zero utility. Composition bounds accumulate across operations, limiting long-term processing capabilities, with epsilon growing as O(sqrt(k)) for k operations even with optimal composition. The curse of dimensionality affects multimedia data with thousands of features, requiring noise proportional to dimensionality, which degrades utility.

Implementation constraints also impose practical limits. Memory requirements for storing noise matrices scale quadratically with feature dimensions, limiting feasible model sizes to under 1 billion parameters. Synchronization overhead in distributed deployments creates bottlenecks for geographically dispersed systems with latency exceeding 100 ms. The framework cannot protect against adversaries with auxiliary knowledge about data distributions, as differential privacy only bounds information leakage through algorithm outputs.

5.2.2. Scalability Challenges for Large-Scale Deployment

Internet-scale deployment introduces challenges in coordination and resource management. Global privacy budget coordination across millions of concurrent requests requires distributed consensus protocols with associated latency and fault-tolerance considerations. Heterogeneous hardware with varying GPU architectures requires platform-specific optimizations, increasing maintenance complexity. Multi-tenant isolation is critical when sharing privacy infrastructure across untrusted applications, requiring careful resource partitioning and accounting.

Data volume challenges emerge at the petabyte scale. Privacy accounting storage grows linearly with request volume, potentially exceeding 100 TB for comprehensive audit logs at internet scale. Real-time analytics on privacy metrics is computationally intensive, necessitating dedicated stream processing infrastructure. Backup and disaster recovery must preserve privacy guarantees while enabling system restoration, complicating traditional approaches.

5.3. Conclusions and Research Impact

5.3.1. Summary of Contributions

This research advances privacy-preserving multimedia processing through three key innovations. The adaptive differential privacy framework allocates privacy budgets based on content sensitivity, achieving 38.7% better utility retention than uniform approaches. Frequency-domain noise calibration preserves perceptual quality while maintaining rigorous privacy guarantees, validated through extensive empirical evaluation. The optimization algorithms solve budget allocation in O(n log n) time, enabling real-time adaptation for streaming multimedia.

Comprehensive experimental validation demonstrates practical viability. The framework processes 312 images/second on commodity hardware while maintaining epsilon = 1.0 differential privacy. Membership inference attacks succeed at only 52.8% rate, approaching theoretical limits. Task accuracy reaches 91.3% of unprotected baselines, sufficient for production deployment.

5.3.2. Implications for National Cybersecurity Infrastructure

The framework supports national priorities in privacy-preserving technologies for critical infrastructure. Government adoption enables privacy-compliant surveillance and

intelligence analysis while protecting civil liberties. Quantifiable privacy guarantees facilitate evidence-based policy development and international cooperation on privacy standards.

Economic implications include competitive advantages in privacy technology markets projected at $190B by 2025. The framework enables GDPR-compliant cloud services accessing European markets and supports privacy-preserving healthcare analytics advancing precision medicine. These capabilities strengthen technological sovereignty by reducing dependence on foreign providers. The research also contributes trained personnel in privacy engineering, addressing workforce shortages and fostering academic-industry partnerships that accelerate technology transfer.

References

1. Y. Zhao, and J. Chen, "A survey on differential privacy for unstructured data content," *ACM Computing Surveys (CSUR)*, vol. 54, no. 10s, pp. 1-28, 2022. doi: 10.1145/3490237
2. J. So, B. Güler, and A. S. Avestimehr, "CodedPrivateML: A fast and privacy-preserving framework for distributed machine learning," *IEEE Journal on Selected Areas in Information Theory*, vol. 2, no. 1, pp. 441-451, 2021.
3. A. K. Singh, and R. Gupta, "A privacy-preserving model based on differential approach for sensitive data in cloud environment," *Multimedia Tools and Applications*, vol. 81, no. 23, pp. 33127-33150, 2022. doi: 10.1007/s11042-021-11751-w
4. Z. Zhou, H. Chen, L. Chen, D. Zhang, C. Wu, X. Liu, and M. K. Khan, "NetDP: In-network differential privacy for large-scale data processing," *IEEE Transactions on Green Communications and Networking*, 2024. doi: 10.1109/tgcn.2024.3432781
5. A. Rahdari, E. Keshavarz, E. Nowroozi, R. Taheri, M. Hajizadeh, M. Mohammadi, and T. Bauschert, "A survey on privacy and security in distributed cloud computing: Exploring federated learning and beyond," *IEEE Open Journal of the Communications Society*, 2025. doi: 10.1109/ojcoms.2025.3560034
6. F. Amiri, G. Quirchmayr, and E. Weippl, "Introducing differential privacy to recommender systems through a self-organizing feature map using a local distance-based methodology," *IEEE Access*, 2025. doi: 10.1109/access.2025.3605563
7. S. Y. Chang, H. C. Wu, K. Yan, S. C. H. Huang, and Y. Wu, "Federated multimedia recommendation systems with privacy protection," In *2024 IEEE International Symposium on Broadband Multimedia Systems and Broadcasting (BMSB)*, June, 2024, pp. 1-7.
8. G. Zhu, X. Li, C. Zheng, and L. Wang, "Multimedia fusion privacy protection algorithm based on IoT data security under network regulations," *Computational Intelligence and Neuroscience*, vol. 2022, no. 1, p. 3574812, 2022.
9. X. Wang, J. Lv, B. G. Kim, C. Maple, B. D. Parameshachari, A. Slowik, and K. Li, "Generative adversarial privacy for multimedia analytics across the IoT-edge continuum," *IEEE Transactions on Cloud Computing*, 2024.
10. B. Liu, M. Ding, S. Shaham, W. Rahayu, F. Farokhi, and Z. Lin, "When machine learning meets privacy: A survey and outlook," *ACM Computing Surveys (CSUR)*, vol. 54, no. 2, pp. 1-36, 2021.
11. R. Xu, N. Baracaldo, and J. Joshi, "Privacy-preserving machine learning: Methods, challenges and directions," *arXiv preprint arXiv:2108.04417*, 2021.
12. A. R. Shahid, and A. Imteaj, "Securing user privacy in cloud-based whiteboard services against health attribute inference attacks," *IEEE Transactions on Artificial Intelligence*, vol. 5, no. 8, pp. 3872-3885, 2024. doi: 10.1109/tai.2024.3352529
13. R. Gupta, and A. K. Singh, "A differential privacy-based secure data sharing model in cloud environment," In *2022 IEEE 6th Conference on Information and Communication Technology (CICT)*, November, 2022, pp. 1-6. doi: 10.1109/cict56698.2022.9997953
14. M. A. Husnoo, A. Anwar, R. K. Chakrabortty, R. Doss, and M. J. Ryan, "Differential privacy for IoT-enabled critical infrastructure: A comprehensive survey," *IEEE Access*, vol. 9, pp. 153276-153304, 2021. doi: 10.1109/access.2021.3124309
15. Z. Wang, Z. Liu, Y. Luo, T. Zhou, J. Qin, and Z. Cai, "PPIDM: Privacy-preserving inference for diffusion model in the cloud," *IEEE Transactions on Circuits and Systems for Video Technology*, 2025. doi: 10.1109/tcsvt.2025.3553514